Neuronal SH2B1 attenuates apoptosis in an MPTP mouse model of Parkinson's disease via promoting PLIN4 degradation

Xiaojuan Han [a,e,1], Yuan Liu [b,c,1], Yan Dai [c], Tianshu Xu [a], Qinghui Hu [c], Xiaolan Yi [c], Liangyou Rui [d], Gang Hu [a,e,**], Jun Hu [b,*]

[a] *Department of Rheumatology and Immunology, Department of Traditional Chinese Medicine, Nanjing Drum Tower Hospital Clinical College of Traditional Chinese and Western Medicine, Nanjing University of Chinese Medicine, Nanjing, 210008, China*
[b] *Department of Orthopedics, the First Affiliated Hospital of Nanjing Medical University, Nanjing, 210029, China*
[c] *Department of Infectious Diseases, the First Affiliated Hospital of Nanjing Medical University, Nanjing, 210029, China*
[d] *Department of Molecular and Integrative Physiology, University of Michigan Medical School, Ann Arbor, MI, USA*
[e] *Department of Pharmacology, Nanjing University of Chinese Medicine, Nanjing, 210023, China*

ARTICLE INFO

ABSTRACT

The incidence of Parkinson's disease (PD) has increased tremendously, especially in the aged population and people with metabolic dysfunction; however, its underlying molecular mechanisms remain unclear. SH2B1, an intracellular adaptor protein, contributes to the signal transduction of several receptor tyrosine kinases and exerts beneficial metabolic effects for body weight regulation; however, whether SH2B1 plays a major role in pathological neurodegeneration in PD has not yet been investigated. This study aimed to investigate the effects of SH2B1 in 1-methyl-4-phenyl-1,2,3,6-tetrahydropyridine (MPTP)–induced PD mice with *Sh2b1* deficiency or neuron-specific *Sh2b1* overexpression. Cellular and molecular mechanisms were elucidated using human dopaminergic neuron SH-SY5Y cells analysed. We found that SH2B1 expression was confirmed to be downregulated in the blood samples of PD patients and in the brains of mice with MPTP-induced chronic PD. *Sh2b1* deficiency caused marked exacerbation of behavioural defects and increased neuronal apoptosis in MPTP-treated mice, whereas restoration of neuron-specific *Sh2b1* expression significantly reversed these effects. Similar results were observed in MPP$^+$-treated SH-SY5Y cells. Mechanistically, upon binding to heat shock cognate 70 (HSC70), SH2B1 promotes HSC70-related recognition and PLIN4 lysosomal translocation and degradation, thus suppressing lipid peroxidation stress in the brains of PD mice. Adeno-associated virus-mediated rescue of neuronal HSC70 expression functionally alleviated the neuropathology of PD in wild-type but not in *Sh2b1*-deficient mice. This is the first study to examine the molecular underpinnings of SH2B1 against MPTP-induced neurodegeneration through cell autonomous promotion of neuronal survival in an *in vivo* PD model. Our findings reveal that SH2B1 antagonizes neurodegenerative pathology in PD via the SH2B1–HSC70–PLIN4 axis.

1. Introduction

Over the past few decades, the number of people diagnosed with Parkinson's disease (PD) has increased tremendously, especially affecting the aged population and people with metabolic dysfunction [1, 2]; however, the molecular mechanisms underlying PD pathology have not been clarified. Recent papers reported that genetic and metabolic regulation abnormalities can cause neurodegenerative diseases and diabetes [3–5]. Based on those observations, the interaction of insulin

and dopamine in the pathogenesis of PD and type 2 diabetes mellitus (T2DM) is becoming a hot spot of research and attention for nearly a decade. PD and T2DM might share similar dysregulated molecular pathways in metabolism networks [6].

Src homology 2 (SH2) B adaptor protein 1 (SH2B1) belongs to a family of adaptor proteins that also includes Src homology 2 B adaptor protein 2 (SH2B2; also known as adaptor protein with PH and SH2 domains, APS) and Src homology 2 B adaptor protein 3 (SH2B3; also known as lymphocyte adapter protein, Lnk) [7]. All three members share characteristic PH and SH2 domains but exhibit different

---

Abbreviations:

αTP	α-tocopherol
AAV	adeno-associated virus
AD	Alzheimer's disease
ANOVA	analysis of variance
AV/PI	annexin V/PI
CASP3	caspase-3
C-CASP3	cleaved caspase-3
CMA	chaperone-mediated autophagy
co-IP	co-immunoprecipitation
DHE	dihydroethidium
DA	dopaminergic
EV	empty vector
FA	fatty acid
HSC70	heat shock cognate 70
IHC	immunohistochemistry
IP	immunoprecipitation
iPSC	induced pluripotent stem cell
IIS	insulin/insulin-like growth factor-1 signalling
IRS	insulin receptor substrate
JAK2	janus kinase 2
KO	knockout
LD	lipid droplet
LC-MS/MS	liquid chromatography-tandem mass spectrometry
LV	lentivirus
MPP	1-methy-4-phenylpyridinium
MPTP	1-methyl-4-phenyl-1,2,3,6-tetrahydropyridine
MS	mass spectrometry
PD	Parkinson's disease
pro-CASP3	procaspase-3
qPCR	real-time quantitative polymerase chain reaction
ROS	reactive oxygen species
SCR	scrambled siRNA
SDS-PAGE	sodium dodecyl sulphate-polyacrylamide gel electrophoresis
SH2	Src homology 2
SH2B1	Src homology 2 B adaptor protein 1
SH2B2	Src homology 2 B adaptor protein 2
SH2B3	Src homology 2 B adaptor protein 3
SEM	standard error of the mean
SNpc	substantia nigra pars compacta
SVZ	subventricular zone
T2D	type 2 diabetes
TH	tyrosine hydroxylase
Tg	transgenic
WB	western blot
WT	wild-type

expression patterns and functions [8,9]. For example, genetic deletion of *Sh2b1,* the gene encoding SH2B1, in mice resulted in severe insulin resistance, obesity, and T2DM [10], whereas that of *Sh2b2* did not alter insulin sensitivity [11]. SH2B1 may also play a critical role in maintaining neuronal differentiation, growth, and reproduction [12]; regulating lifespan and metabolic homeostasis [13]; and promoting cell proliferation in lung adenocarcinoma [14].

Moreover, SH2B1 is expressed ubiquitously in various tissues, including the brain [8], indicating that it may play an important regulatory role in brain physiology and pathology. Intriguingly, our previous study has revealed that neuron-specific restoration of SH2B1 expression can reverse obesity and T2D phenotypes in *Sh2b1*-null mice [8]. SH2B1 can enhance neurite outgrowth and accelerate the maturation of human induced pluripotent stem cell (iPSC)-induced neurons [12]. In diseased states, SH2B1 acts to inhibit Aβ accumulation and has a protective role in the pathogenesis of Alzheimer's disease (AD) [15]. However, whether SH2B1 plays a major role in pathological neurodegeneration in PD has not yet been investigated.

In the present study, using our previously established *Sh2b1* knockout (KO) mice and neuronal *Sh2b1* transgenic (Tg) mice [8,16,17] and 1-methyl-4-phenyl-1,2,3,6-tetrahydropyridine (MPTP) PD *in vivo* and 1-methy-4-phenylpyridinium (MPP)$^+$ *in vitro* models [18–20], we investigated whether SH2B1 were involved in the progression of PD and further observed what is the molecular basis for the observed effects of SH2B1 in neurodegenerative pathology in PD.

2. Materials and methods

2.1. Blood sample collection

All healthy control subjects and PD patients were recruited from the First Affiliated Hospital of Nanjing Medical University. All procedures involving the use of human tissues were approved by the Ethics Committee of the First Affiliated Hospital of Nanjing Medical University (Ethical Application Ref: 2020-SR-063), and informed consent was obtained from each participant.

Blood samples were collected from the peripheral veins of 29 control participants and 26 PD patients. There were 15 male and 14 female

healthy participants, with an average age of 69.1 ± 5.9. There were 17 male and 9 female PD patients, with an average age of 69.5 ± 4.3. PD patients were classified according to Hoehn–Yahr staging system as follows: stage I (n = 3), stage II (n = 5), stage III (n = 9), stage IV (n = 7), and stage V (n = 2). No statistically significant difference in age and gender was found between the two groups. The relative expression level of SH2B1 mRNA in the blood samples was detected by real-time quantitative polymerase chain reaction (qPCR).

2.2. Animals

Four-month-old male *Sh2b1* knockout (KO) mice and neuronal-specific *Sh2b1* transgenic (Tg) mice were donated by Professor Liangyou Rui (Department of Molecular and Integrative Physiology, University of Michigan Medical School, Michigan, USA). *Sh2b1* Tg mice were generated as previously reported [8]. In brief, recombinant *Sh2b1* was specifically expressed in neural tissues under the control of the NSE promoter/rat GH enhancer. Full-length rat *Sh2b1β* cDNA was inserted into a transgenic vector at the 3′-end of the NSE promoter/GH enhancer sequences. The *Sh2b1* transgene construct was microinjected into F2 mouse oocytes (C57BL/6 × SJL), and the oocytes were surgically transferred into recipients to generate heterozygous *Sh2b1* Tg animals. This experiment was performed at the University of Michigan Transgenic Animal Model Core.

All mice were generated and maintained on a congenic C57BL/6 background. Age-matched littermate wild-type (WT) male mice were purchased from the Laboratory Animal Center of Nanjing Medical University (Nanjing, China) and used as controls. Mice were housed on a 12-h light/12-h dark cycle and had free access to pellet food and water under specific pathogen-free conditions at 24 ± 2 °C in the Animal Resource Centre of the Faculty of Medicine, Nanjing Medical University. Mice were deeply anaesthetised with sodium pentobarbital (50 mg/kg, intraperitoneal [i.p.]), blood samples were collected, and the animals were perfused.

The animal experiments in this study were performed in accordance to the Guide for the Care and Use of Laboratory Animals (National Institutes of Health, United States) and the ethical regulations of the Nanjing Medical University (No. IACUC-1601153). All efforts were

made to reduce the number of animals used and to minimise animal suffering.

2.3. MPTP/p-induced PD mouse model and in vivo experimental treatments

Four-month-old male mice of each genotype (WT, *Sh2b1* KO, and *Sh2b1* Tg) were divided into the control and MPTP plus probenecid (MPTP/p)-treated groups. The chronic MPTP treatment protocol was performed as previously described [21]. In brief, 20 mg/kg MPTP (#M − 0896, Sigma-Aldrich, St. Louis, MO, USA) dissolved in saline, and 250 mg/kg probenecid dissolved in dimethyl sulphoxide was added. This solution was injected subcutaneously at 1 h intervals every 3.5 days for five weeks. Control mice were treated with saline and probenecid.

A mouse recombinant *Sh2b1* plasmid was inserted into a packaging vector to generate an adeno-associated virus (AAV-m-*Sh2b1*-hSyn promoter MCS EGFP 3FLAG SV40 PolyA, serotypes 9, 1×10^{13} vg/mL, GOSE0150140, GeneChem, Shanghai, China). A mouse recombinant *Hspa8* plasmid was inserted into a packaging vector to generate a lentivirus (LV-m-*Hspa8*-3xflag-ZsGreen-PURO, 2×10^{9} TU/mL, HH20190411RFF-LP01, HanBio, Shanghai, China).

For microinjection, anaesthetised mice were placed in a stereotaxic apparatus and injected with 1.0 μL of AAV/LV using a glass electrode (at the following coordinates relative to bregma: −3.0 mm A/P, ± 1.3 mm M/L, and −4.5 mm D/V) at a rate of 0.20 μL/min, after which the needle was left in place for 2 min as previously described [22]. The MPTP-induced PD mouse models were established two weeks after virus microinjection.

2.4. Cell culture and treatment

Authenticated human dopaminergic (DA) neuron SH-SY5Y cells were purchased from the Shanghai Institute of Cell Biology (Shanghai, China), cultured at 37 °C in a 5% (v:v) CO_2 atmosphere, and used at passages 4–14. To induce neuronal damage, cells were incubated with ultrapure MPP^+ (200 mM; #D048, Sigma-Aldrich, St. Louis, MO, USA) for 24 h at 37 °C.

2.5. Lipid droplet (LD) staining and flow cytometry analysis

BODIPY$^{493/503}$ staining was performed as previously described [21]. For dihydroethidium (DHE) staining, live cells were incubated with 0.5 mg/mL DHE (#D11347, Invitrogen, Life Technologies Corporation, Carlsbad, CA, USA) in PBS for 30 min at 37 °C, washed in PBS and fixed in 3.5% PFA for 10 min, and washed and counterstained with Hoechst 33342 (#B2261, Sigma-Aldrich, St. Louis, MO, USA) for 10 min.

For the BODIPY$^{581/591}$ C11 lipid peroxidation assay, live cells were incubated with or without 2 μM BODIPY$^{581/591}$ C11 (#D3861, Invitrogen, Life Technologies Corporation, Carlsbad, CA, USA) for the last 30 min, washed with PBS, and live imaged in PBS using a Zeiss LSM 880 microscope. Images were obtained in both the green and red channels. Relative lipid peroxidation was determined by the ratio of green fluorescence intensity to red fluorescence intensity in background-subtracted images using Image J software (NIH, Bethesda, MD, USA).

Apoptosis cells was assessed by staining cells with Annexin V/PI (AV/PI) at 37 °C for 30 min. The cells were then washed with PBS and resuspended in cold PBS containing 1% FBS and analysed by flow cytometry (Guava EasyCyte Plus System, Millipore, Billerica, MA, USA).

2.6. Cell transfection

An siRNA targeting *SH2B1*, a scrambled siRNA (SCR), *SH2B1* plasmid or empty vector (EV; Genepharma, Shanghai, China) was transfected into SH-SY5Y cells using Lipofectamine RNAiMAX (#13778100, Invitrogen, Life Technologies Corporation, Carlsbad, CA, USA) in OptiMEM reduced serum medium (Gibco) according to the

manufacturer's instructions. For *SH2B1* plasmid transfection, SH-SY5Y cells were seeded into six-well plates at a density of 5×10^5 per well in complete cell culture medium. After 24 h, the cells were transfected with plasmids expressing Flag-*SH2B1* and exposed to the indicated stimuli 48 h later. pcDNA3.1-GFP-*SH2B1* plasmid and/or LV-*shHSPA8* was transfected into SH-SY5Y cells using Lipofectamine 3000 (#L3000-015, Invitrogen, Life Technologies Corporation, Carlsbad, CA, USA) according to the manufacturer's instructions. The cells were collected for Western blot (WB) analysis or coimmunoprecipitation (Co-IP) analysis 48 h after transfection.

2.7. Unbiased stereology

The total numbers of tyrosine hydroxylase (TH)$^+$ neurons and Nissl-stained neurons were quantified by unbiased stereology using the optical fractionator method as previously described [22,23].

2.8. WB analysis and Co-IP

The protocol used for WB analysis was as reported previously [23]. Briefly, brain tissues and cells were homogenised in RIPA lysis buffer. A 30-μg aliquot of protein from each sample was separated using sodium dodecyl sulphate-polyacrylamide gel electrophoresis (SDS-PAGE; 10–12%) and transferred onto PVDF membranes (IPVH00010, Millipore, Billerica, MA, USA) blocked with 10% nonfat dry milk in Tris-buffered saline with Tween-20 (#T104863, Aladdin, Shanghai, China). Membranes were probed with primary antibodies overnight at 4 °C and incubated with horseradish peroxidase-conjugated goat anti-mouse (#31430, Invitrogen, Life Technologies Corporation, Carlsbad, CA, USA) or rabbit (#31460, Invitrogen, Life Technologies Corporation, Carlsbad, CA, USA) IgG secondary antibodies (1:2000). Antibodies to SH2B1 (#12226-1-AP, 1:1000, Proteintech Group, Chicago, USA), TH (#ab6211, 1:1000, Abcam, Cambridge, MA, USA), procaspase-3 (pro-CASP3; #48686, 1:800, Signalway Antibody, College Park, Maryland, USA), caspase-3 (CASP3; #9662s, 1:800, Cell Signaling Technology Inc., Danvers, MA, USA), PLIN4 (#13776, 1:1000, Novus Biologicals, Littleton, CO, USA), and ACTB (#sc-47778, 1:2000, Santa Cruz, CA, USA) were used. Detection was performed using an Image-Quant LAS 4000 mini luminescent image analyser (Uppsala, Sweden). Band intensity was quantified using ImageJ software (NIH, Bethesda, MD, USA).

For Co-IP, cells were collected, lysed with lysis buffer on ice for 30 min, and centrifuged at $16000 \times g$ at 4 °C for 15 min. The supernatant fractions were collected, incubated with the appropriate antibodies at 4 °C overnight, and precipitated with protein A/G-agarose beads (#sc-2003, Santa Cruz, CA, USA) for 4 h at 4 °C. Antibodies to SH2B1 (#12226-1-AP, 1:1000, Proteintech Group, Chicago, USA), Heat shock cognate 70 (HSC70) (#sc-7298, 1:1000, Santa Cruz, CA, USA), and ACTB (#sc-47778, 1:2000, Santa Cruz, CA, USA) were used. The beads were washed with lysis buffer thrice by centrifugation at $1000 \times g$ at 4 °C. The immunoprecipitated proteins were separated by SDS-PAGE, and WB analysis was performed with the indicated antibodies.

2.9. Liquid chromatograph – tandem mass spectrometry (LC-MS/MS)

Anti-SH2B1 immunoprecipitated protein (300 μg for each sample) was digested according to reported procedure [24]. Mass spectrometry (MS) experiments were performed with a Q Exactive mass spectrometer. Digested peptides were packed to a C18-reversed-phase column with mobile phase A (0.1% formic acid and 2% acetonitrile) and chromatographed with mobile phase B (0.1% formic acid and 80% acetonitrile) over 120 min. MS spectra were collected using a data-dependent top10 method, which dynamically chooses the most abundant precursor ions from the survey scan (300–1800 m/z) for HCD fragmentation. MS data were analysed using MaxQuant software version 1.3.0.5 and were searched against the UniProtKB database.

2.10. Histological analysis, immunohistochemistry (IHC), and immunofluorescence

For IHC or immunofluorescence staining, brain sections were dehydrated in gradient alcohol solutions after post-fixation. As previously described [22], brain tissue encompassing the entire substantia nigra pars compacta (SNpc) was cut into 30-μm slices with a cryostat (M1950-1-0-0-1-1, Leica Microsystems, Nussloch, Germany), incubated with 0.3% Triton X-100 in PBS for 15 min, and blocked with 5% goat serum (#16210-064, Invitrogen, Life Technologies Corporation, Carlsbad, CA, USA) for 1 h at 24 ± 2 °C. Then, the sections were incubated with specific primary antibodies at 4 °C overnight. Antibodies to SH2B1 (#12226-1-AP, 1:250, Proteintech Group, Chicago, USA), TH (#ab6211, 1:800, Abcam, Cambridge, MA, USA), GFAP (#MAB360, 1:800, Millipore, Billerica, MA, USA), IBA-1 (#019–1974, 1:1000, Wako Pure Chemical Industries, Ltd, Osaka, Japan), cleaved caspase-3 (C-CASP3; #40500, 1:400, Signalway Antibody, College Park, Maryland, USA), HSC70 (#ab19136, 1:500, Abcam, Cambridge, MA, USA) and PLIN4 (#13776, 1:400, Novus Biologicals, Littleton, CO, USA) were used.

For immunofluorescence, the sections were washed and incubated with Alexa Fluor 488-conjugated donkey anti-mouse IgG (#A21202, 1:800, Invitrogen, Life Technologies Corporation, Carlsbad, CA, USA) or Alexa Fluor 555-conjugated goat anti-Rat IgG (#A21432, 1:800, Invitrogen, Life Technologies Corporation, Carlsbad, CA, USA) for 1 h. After a final wash with PBS, the sections were mounted onto glass slides, and ProLong gold anti-fade reagent containing DAPI (#P36931, Invitrogen, Life Technologies Corporation, Carlsbad, CA, USA) was applied for visualization of the nuclei. For IHC, the slides were incubated with streptavidin-HRP (#31430, 31460, 31402, 1:1000, Invitrogen, Life Technologies Corporation, Carlsbad, CA, USA) for 40 min and stained with DAB (#GK500705, Gene Tech, Shanghai, China).

2.11. Behavioural analyses

Behavioural analyses were carried out as previously described [25]. For the rotarod test, mice were accustomed to the rotarod with an accelerated speed from 4 to 40 rpm over 5 min for 3 trials per day in the next 3 consecutive days. The latency to fall was measured using Rotarod Analysis System (Jiliang, Shanghai, China). For the pole test, a vertical wooden pole (rough, height 50 cm, diameter 1 cm) was used. All mice were acclimatized to the apparatus 3 times by placing head up before testing and then tested for 3 times in the next day. The climbing down time (for the mouse to reach the floor) and the turning time (for the mouse to turn completely head downward) were recorded.

2.12. RNA reverse transcription and real-time qPCR

Total RNA was extracted with TRIzol reagent (#15596026, Invitrogen, Life Technologies Corporation, Carlsbad, CA, USA). Total RNA (1 μg) from each sample was reverse transcribed into cDNA and amplified using a PrimeScript™ 1st Strand cDNA Synthesis Kit (#6110A, TaKaRa Biotechnology, Dalian, China) according to the manufacturer's directions. qPCR was performed using SYBR Green qPCR Master Mix kit (#A021A, TaKaRa Biotechnology, Dalian, China) and the following primers (Table 1) on the ABI 7300 StepOne™ Fast Real-Time PCR System (Applied Biosystems, Foster City, CA, USA). mRNA levels were determined by normalising to the level of GAPDH in the experimental samples to that in the control samples as previously described [23].

2.13. Statistical analysis

Statistical analysis was performed using GraphPad Prism 7 software (GraphPad Software, Inc., La Jolla, CA, USA). Data are presented as the mean ± standard error of the mean (SEM) and were collected and analysed in a blinded manner. Differences between groups were

Table 1
Primer sequences for real-time quantitative PCR.

Gene	Forward sequence (5′-3′)	Reverse sequence (5′-3′)
Human		
SH2B1	GGCTGGGCGCTCGTC	GTGGGGCACAAAGAGGGAG
GAPDH	CCGCATCTTCTTTTGCGTCG	ATCCGTTGACTCCGACCTTC
Mouse		
Sh2b1	CGAGAGGGCAGCAGATAGTT	GACCCGATCCTAGTCGTTGG
Sh2b2	AACCCGACCTACGACACG	CAGGAGCAGGCGACACTT
Sh2b3	CTCCCTCAGGACAGTTGC	TGCTGTAACCCAGAGTCCTT
Gpx8	TGGCTTTTCCGTGCAATCAG	TTCTGCTTCCGGCCCTAAAA
Sod3	AAGACAATCCCACAAGCCCC	TGGGGTGGGCGATATTTCAG
Cat	AGAGGAAACGCCTGTGTGAG	GCGTGTAGGTGTGAATTGCG
Acsbg1	CAGCGGAAAAACCAGGAAGAA	GCATTCACCGAAGACAGTGC
Dbi	GAGCGGAACTTTTTCCCTTGC	TTGTTCCACGAGTCCCACTT
Gapdh	GAAGGTCGGTGTGAACGGAT	CAATCTCCACTTTGCCACTGC

analysed using Student's *t*-test, and those among groups using one-way analysis of variance (ANOVA) with Tukey's post-hoc test. Two-way ANOVA with Tukey's multiple comparisons test was used to analyse the effect of two nominal predictor variables. $P < 0.05$ were considered significant. The number of technical and biological replicates of individual experiments and the corresponding statistical tests are indicated in the figure legends.

3. Results

3.1. SH2B1 expression is decreased in PD patients and PD mouse model

The relative expression level of *SH2B1* mRNA was significantly lower in the blood samples of PD patients than in those of healthy participants (Fig. 1a). Interestingly, in both the midbrain and striatum of mice, *Sh2b1* was more highly expressed than *Sh2b2* and *Sh2b3* (Fig. 1b). In the SNpc, the region involved in PD pathology, SH2B1 was expressed not only in TH$^+$ DA neurons but also in GFAP$^+$ astrocytes and IBA-1$^+$ microglial cells (Fig. 1c). The mRNA level of *Sh2b1* in the midbrain were significantly reduced in MPTP/p-induced chronic PD mice compared with control mice (Fig. 1d).

Consistently, immunoblot analysis demonstrated the marked down-regulation of SH2B1 expression in both midbrain and striatum homogenates of MPTP/p-induced PD mice compared with those of saline-treated controls (Fig. 1e and f). Confocal imaging further confirmed that SH2B1 expression was lower in the brains of MPTP/p-treated mice than in those of control mice, especially in TH$^+$ neurons in the SNpc, in which marked TH$^+$ neuron loss was also observed (Fig. 1g). Collectively, these data suggest that reduced expression of SH2B1 in the brain (especially in TH$^+$ neurons) is associated with PD development.

3.2. SH2B1 alteration changes behavioural dysfunction and DA neuron loss in MPTP/p-induced PD mice

To clarify the role of SH2B1 expression in the pathogenesis of PD, we evaluated whether *Sh2b1* alteration changes parkinsonism in mice. We found that both the number of TH$^+$ DA neurons and TH protein levels are decreased in the SNpc of MPTP-injected mice compared with saline-treated controls, confirming that the model was successfully established.

To assess parkinsonism-related behaviour, we employed the rotarod test and pole test, which are used to evaluate coordination and muscle strength. No differences in baseline behavioural performance were observed between *Sh2b1* KO mice and WT controls (Fig. 2a and b). *Sh2b1* KO exacerbated the MPTP-induced impairment of motor coordination, as evidenced by the decrease in latency to fall (Fig. 2a). In the pole test, the latency to climb down the pole was increased in MPTP-treated WT mice compared with saline-treated WT mice (Fig. 2b), and the latency to turn and climb down the pole was further prolonged in MPTP-treated *Sh2b1* KO mice compared (Fig. 2a and b). Furthermore, MPTP-injected mice presented severe nigral TH$^+$ neuron loss, which was
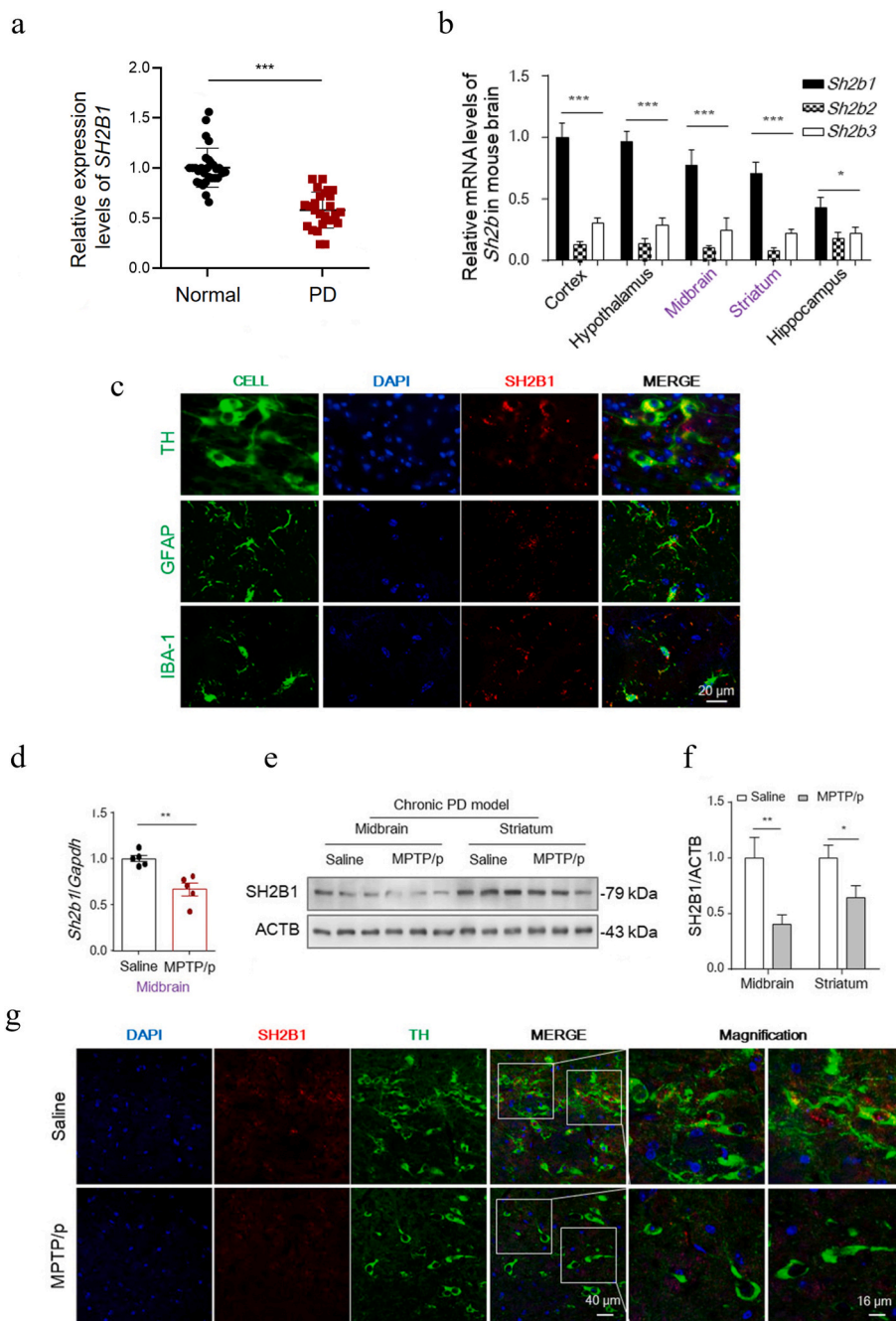
Fig. 1. SH2B1 expression was decreased in PD patients and PD mice. (a) *SH2B1* mRNA expression in the venous blood samples of 26 patients with PD was reduced. (b) *Sh2b1*, *Sh2b2*, and *Sh2b3* mRNA levels in the different brain regions of four-month-old C57BL/6 mice. (c) Representative images showing SH2B1$^+$ cells expressing markers of neurons (TH, top panel), astrocytes (GFAP, middle panel), and microglia (IBA-1, bottom panel) in mouse brain sections containing SNpc. Scale bar, 20 μm. (d) *Sh2b1* mRNA levels in the midbrains of both saline- and MPTP/p-treated mice. (e and f) Midbrain and striatum SH2B1 levels in saline- and MPTP/p-treated mice were analysed by immunoblotting (e) and quantified (f). (g) Immunostaining data showing SH2B1 intensity in TH$^+$ neurons in the SNpc of saline- and MPTP/p-treated mice. Scale bar, 40/16 μm. Data are presented as the mean ± SEM of three independent experiments. (a) n = 29 healthy subjects, n = 26 patients with PD; (b–d) n = 5–6 mice per group, (e–g) n = 3 mice per group. Analysed by (a and d) two-tailed Student's *t*-test or (b and f) one-way ANOVA with Tukey's post hoc test (*$P < 0.05$; **$P < 0.01$; ***$P < 0.001$; ns, not significant).

exacerbated in *Sh2b1* KO mice compared with WT controls (Fig. 2e and f). Moreover, TH protein levels in midbrain extracts were much lower in MPTP-treated *Sh2b1* KO mice than in MPTP-treated WT mice (Fig. 2i and j).

To confirm the role of SH2B1 in PD, we tested whether cDNA recombination-induced neuron-specific *Sh2b1* (*Sh2b1*$^{tg/tg}$) overexpression can reduce MPTP-induced damage. We found that MPTP/p-induced behavioural deficits are markedly reversed by neuron-specific *Sh2b1* overexpression, as shown by improvement in performance in the rotarod test (Fig. 2c) and the pole test (Fig. 2d). *Sh2b1* overexpression significantly alleviated the MPTP/p-induced loss of DA neurons and decreased TH protein levels in the substantia nigra (Fig. 2g, h, k and l). Collectively, these results suggest that SH2B1 is a key regulator in PD, as *Sh2b1* KO and neuronal *Sh2b1* overexpression aggravated and alleviated pathology, respectively, in the MPTP/p-induced PD mouse model.

The observed co-expression of SH2B1 and TH led us to hypothesise that the exacerbation of parkinsonism induced by *Sh2b1* KO involved TH $^+$ neurons but not glial cells. To confirm this hypothesis, we evaluated whether overexpressing *Sh2b1* in neurons could reverse MPTP-induced neurotoxicity in *Sh2b1* KO mice. In preliminary experiments, we observed that the administration of AAV-*Sh2b1* for two weeks achieved sufficient protein expression. As expected, stereotaxic injection of AAV-*Sh2b1* into the SNpc significantly increased SH2B1-GFP expression, mostly in TH$^+$ cells (Fig. 2m). Moreover, we found that the acceleration of TH$^+$ neuron loss and the decrease in TH levels in the SNpc were relatively reduced in AAV-*Sh2b1*-injected mice compared to AAV-*vector*-injected controls (Fig. 2n, o).
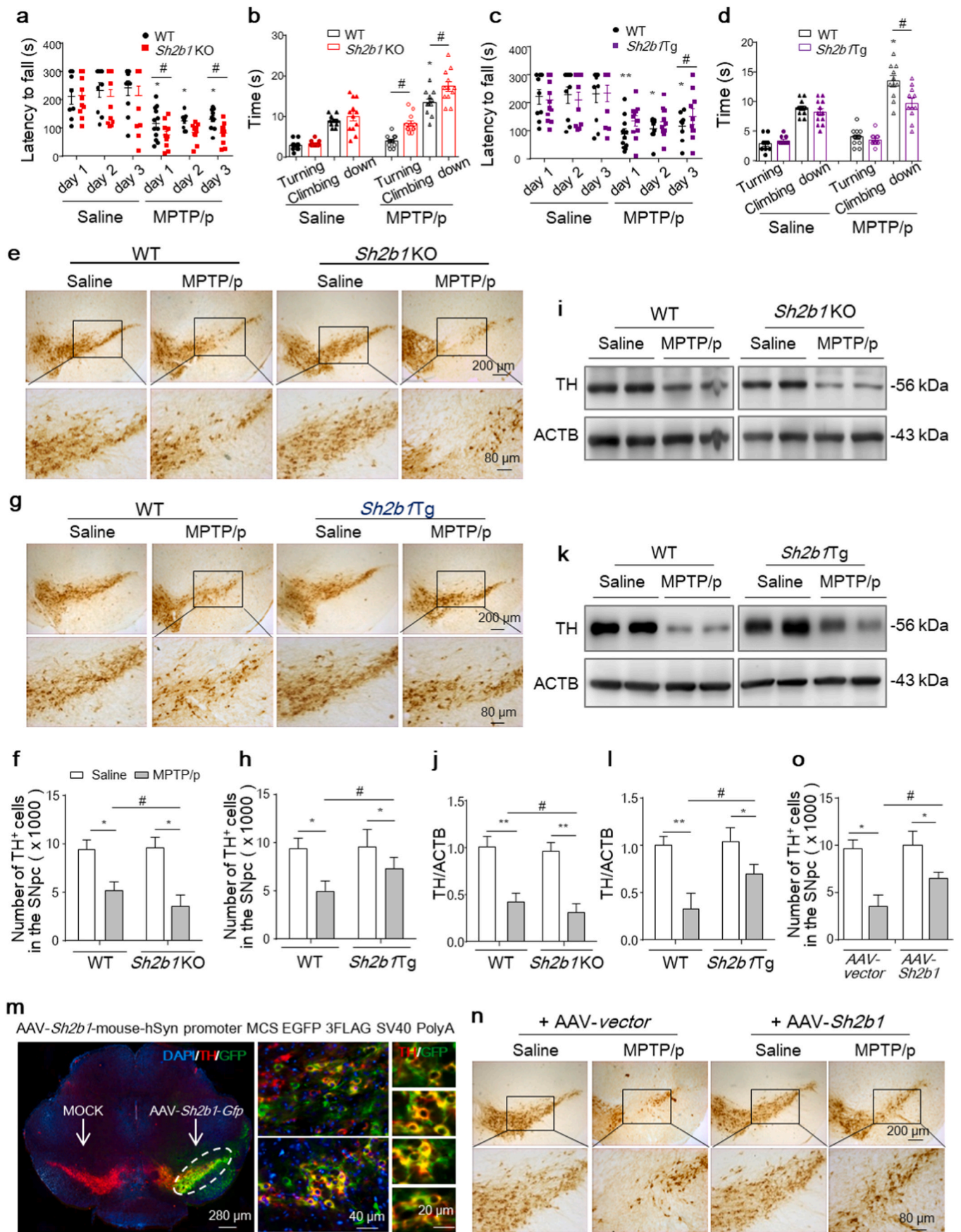
Fig. 2. SH2B1 deficiency exacerbates DA neuron loss in PD mice, whereas its overexpression reverses this effect. (a–d) Behavioural results of four-month-old WT, *Sh2b1* KO, and *Sh2b1* Tg mice after saline or MPTP injection: (a and c) rotarod test, (b and d) pole test. (e–h) Representative images and quantification of TH$^+$ neurons in each group. Scale bar, 200/80 μm. (i–l) WB analysis and quantification of TH protein levels in the SNpc. (m–o) Four-month-old *Sh2b1*$^{-/-}$ mice were stereotaxically injected with AAV-*Sh2b1* into the SNpc two weeks before MPTP administration. AAV-*vector* was used as the control. (m) IHC results confirm that AAV-*Sh2b1* (GFP) is expressed, mainly in TH$^+$ neurons (red). Scale bar, 280/40/20 μm. Representative images (n) and quantification (o) of TH$^+$ neurons in each group. Scale bar, 200/80 μm. Data are presented as the mean ± SEM of three independent experiments. (a–d) n = 9–11 WT mice treated with saline, n = 10–12 WT mice treated with MPTP, n = 12–13 *Sh2b1* KO mice treated with saline, n = 11–12 *Sh2b1* KO mice treated with MPTP, n = 11–12 *Sh2b1* Tg mice treated with saline, n = 10–12 *Sh2b1* Tg mice treated with MPTP; (e–o) n = 5–6 mice per group. Analysed by (a and c) two-way ANOVA with Tukey's multiple comparisons test or (b, d, f, h, j, l and o) one-way ANOVA with Tukey's post hoc test (*$P < 0.05$, **$P < 0.01$ versus saline group; $^#P < 0.05$ versus MPTP/p-treated WT group). . (For interpretation of the references to colour in this figure legend, the reader is referred to the Web version of this article.)

◀━━━━━━━━━━━

3.3. SH2B1 suppresses MPTP/p-induced neurodegeneration by inhibiting TH$^+$ neuronal apoptosis and protects SH-SY5Y cells against MPP$^+$-induced cell death

We further determined whether the loss of DA neurons in *Sh2b1* KO mice is due to an increase in apoptosis. We observed an increase in the number of active CASP3$^+$ cells in the brain slices of MPTP-injected mice, which was aggravated in MPTP-treated *Sh2b1* KO mice and alleviated in MPTP-treated *Sh2b1* Tg mice (Fig. 3a and b). We also found a higher number of TUNEL$^+$ cells, accompanied by a greater reduction in the number of TH$^+$ neurons (Fig. 3c and d), in MPTP-treated *Sh2b1* KO mice than in MPTP-treated WT mice. However, these changes were significantly alleviated in MPTP-treated *Sh2b1* Tg mice.

To gain insight into the potential function of SH2B1 in DA neurons, we knocked down and overexpressed *SH2B1* in SH-SY5Y cells using siRNA-mediated gene silencing and plasmid-mediated gene expression, respectively. SH-SY5Y cells were infected with *SH2B1* siRNA (or SCR) or *SH2B1* plasmid (or EV). To determine whether SH2B1 promotes neuronal survival, SH-SY5Y cells with silenced or overexpressed *SH2B1* were treated with MPP$^+$, a toxin that specifically affects DA neurons, and cell viability was measured. *SH2B1* silencing and overexpression significantly deteriorated and alleviated the reduction in the viability of MPP$^+$-treated SH-SY5Y cells, respectively (Fig. 3e). Moreover, *SH2B1* silencing significantly increased MPP$^+$-induced apoptosis, whereas its overexpression protected SH-SY5Y cells from MPP$^+$-induced apoptosis (Fig. 3f–i).

3.4. SH2B1 protects SH-SY5Y cells from MPP$^+$-induced apoptosis via HSC70

We investigated the proteins interacting with SH2B1 (Fig. 4a and b) and identified HSC70 as the major SH2B1 binding protein (Fig. 4c). This was confirmed by WB analysis and IP (Fig. 4d and e). MPP$^+$ weakened the binding between SH2B1 and HSC70 and reduced SH2B1 expression but not HSC70 expression (Fig. 4e). This interaction was further confirmed by colocalization analysis by confocal imaging, which showed that the SH2B1 fluorescence signal was colocalised with HSC70 in cultured SH-SY5Y cells (Fig. 4f). We subsequently determined whether HSC70 functionally affects SH2B1-triggered neuroprotective events. A reduction in HSC70 expression significantly blunted the anti-apoptotic effect of SH2B1 overexpression on MPP$^+$-stimulated SH-SY5Y cells (Fig. 4g–j).

3.5. PLIN4/LDs function downstream of the SH2B1/HSC70 axis and partially contribute to SH2B1-mediated neuroprotection

A recent study has suggested that LD-related lipotoxicity participates in PD pathology [26]. Perilipin family members (PLIN1-5), the surrounding proteins of LDs, are regarded as the most important regulator of LDs, facilitating LD movement and cellular signalling interactions [27,28]. We have previously reported that the PLIN4/LD/mitophagy axis has a crucial role in neurodegeneration owing to MPTP/MPP$^+$ insult, indicating PLIN4/LDs as a potential biomarker and therapeutic target for PD [21].

In this study, we found that PLIN4 was colocalised with HSC70 and

that MPP$^+$ challenge increased colocalization in lysosomes, which was remarkably alleviated by *SH2B1* overexpression (Fig. 5a and b). Knockdown of *SH2B1* increased PLIN4 intensity in MPP$^+$-treated SH-SY5Y cells (Fig. 5c and d), whereas its overexpression reduced it (Fig. 5e and f). Finally, we confirmed that *PLIN4* knockdown partially alleviates the acceleration of apoptosis induced by *SH2B1* siRNA in MPP$^+$-treated SH-SY5Y cells (Fig. 5g and h). These results support that PLIN4 acts downstream of SH2B1/HSP70.

Increased expression of PLIN4, as a perilipin, mainly promotes intracellular LD deposition. In the context of PD, a compensatory increase in neuronal activity combined with MPTP/p-MPP$^+$ can aggravate reactive oxygen species (ROS) generation by damaging the mitochondrial respiratory chain. Thus, we speculated that the deposition of LDs and an increase in mitochondrial ROS generation may mutually promote lipid peroxidation and exacerbate ROS stress to induce apoptosis.

To evaluate this hypothesis, we measured lipid peroxidation in cells and found an increase in the levels of peroxidised lipids in both LDs and the surrounding membranes in cells upon treatment with MPP$^+$. This increasement was aggravated by *SH2B1* knockdown, indicating that lipid peroxidation in SH-SY5Y cells was indeed increased (Fig. 6a, c). Additionally, an increase in DHE fluorescence was observed in cultured SH-SY5Y cells treated with MPP$^+$, and this increase was aggravated by *SH2B1* knockdown (Fig. 6b, d), indicating that cellular oxidative stress levels were increased in these cells. A further reduction in cellular oxidation was observed when SH-SY5Y cells were treated with MPP$^+$ plus α-tocopherol (α-TP), a lipid-soluble antioxidant that can block lipid peroxidation (Fig. 6b, d). Treatment with α-TP also partially reversed the *siSH2B1*-mediated acceleration of MPP$^+$-induced cell apoptosis (Fig. 6e and f).
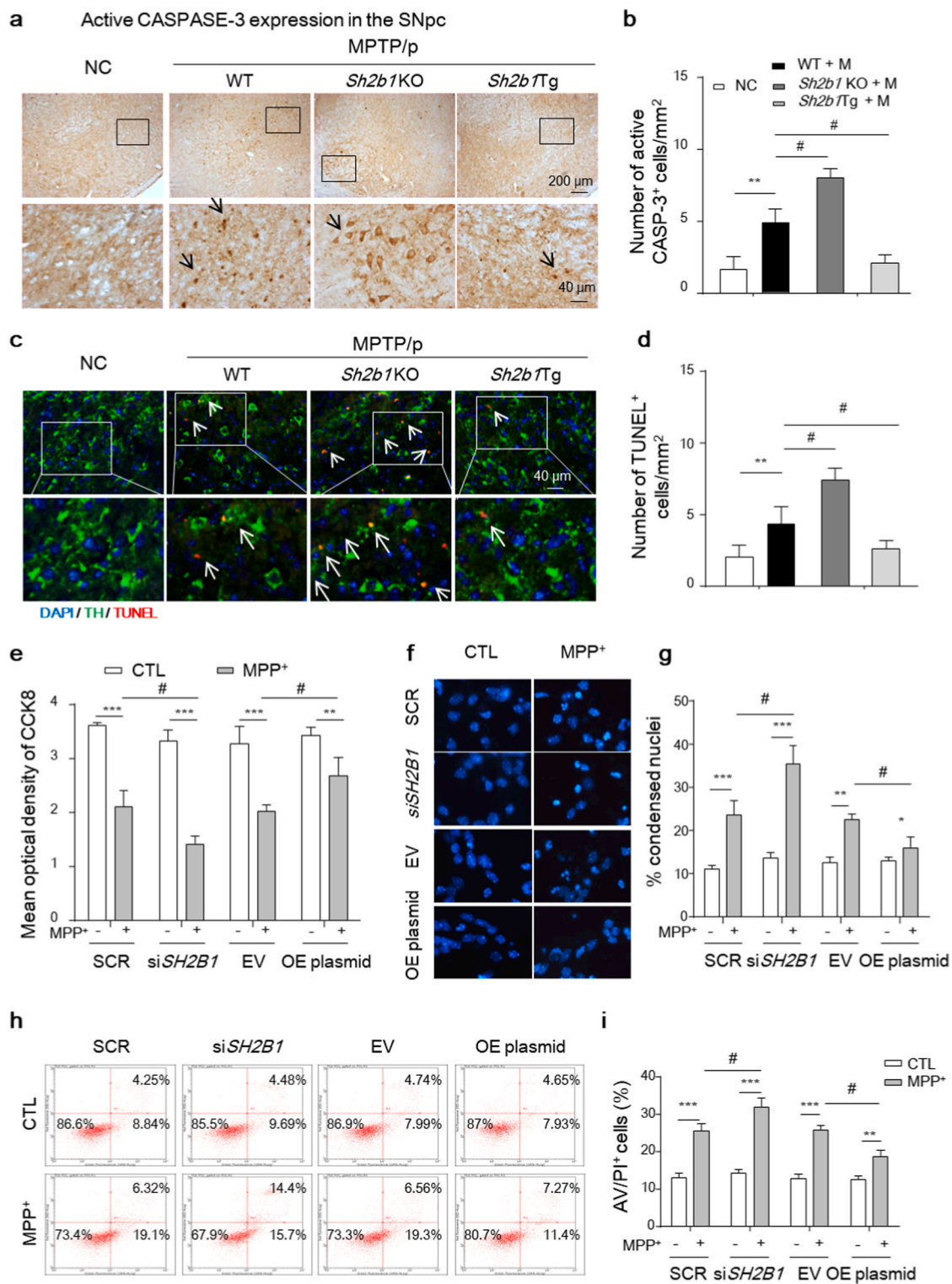
3.6. SH2B1 deficiency exacerbates PLIN4/LD deposition and amplifies lipid oxidative stress in response to MPTP

The aforementioned *in vitro* findings suggest that the effects of SH2B1 in PD are related to PLIN4/LDs/ROS generation; thus, we confirmed this *in vivo*. Immunoblot analysis revealed that PLIN4 levels are increased in the midbrains of MPTP-treated mice and that this increase is exacerbated in *Sh2b1* KO mice and alleviated in neuronal-specific *Sh2b1*-overexpressing mice (Fig. 7a and b). Confocal imaging showed that MPTP treatment resulted in an increase in PLIN4 aggregation in the SNpc, especially in the remaining TH$^+$ neurons (Fig. 7c and d). MPTP-induced PLIN4 aggregation was further aggravated in *Sh2b1* KO mice compared with WT mice, accompanied with exacerbation in TH$^+$ neuron loss (Fig. 7c). Regarding the lipid oxidation pathway, *Sh2b1* KO significantly accelerated the MPTP-induced downregulation of genes that protect against the toxic effects of free fatty acids (*Gpx8*), neutralise superoxide radicals (*Sod3*) and hydrogen peroxide (*Cat*), and are involved in fatty acid (FA) metabolism (*Acsbg1 and Dbi*; Fig. 7e).

### 3.7. Restoration of HSC70 expression alleviates MPTP-induced neurodegeneration in an SH2B1 dependent manner

We found that LV-*Hspa8* injection increased HSC70 levels in the midbrain, which subsequently alleviated the MPTP-induced loss of TH$^+$ neurons (Fig. 8a and b) and the reduction in TH levels but not in *Sh2b1*

Fig. 3. SH2B1 deficiency exacerbates apoptosis of TH $^+$ cells (*in vivo*) and SH-SY5Y cells (*in vitro*). (a and b) Representative images of active CASP3 immunoreactivity showing apoptotic cells (brown) labelled by black arrowheads in the SNpc of the indicated mice. Quantification of active CASP3$^+$ cells in (b) with 3–5 coronal sections per brain (5–10 sections per area). Scale bar, 200/40 μm. (c and d) Representative images of TUNEL staining revealed apoptotic TH$^+$ neurons in the SNpc of the indicated mice. Scale bar, 40 μm. The average number of apoptotic cells in the SNpc is shown (d). (e–i) SH-SY5Y cells infected with *SH2B1* siRNA (or SCR) or *SH2B1* plasmid (or EV) were treated with (or without) MPP$^+$ (200 μM, 24 h). (e) Cell viability was measured using the CCK8 assay. (f and g) Treated cells were fixed for Hoechst staining. Scale bar, 20 μm. (h and i) Cell apoptosis was measured using AV/PI staining. Data are presented as the mean ± SEM of three independent experiments. (a–i) n = 5–6 per group. Analysed by (b, d, e, g and i) one-way ANOVA with Tukey's post hoc test (*$P < 0.05$; **$P < 0.01$; ***$P < 0.001$ versus NC group or vehicle; #$P < 0.05$ versus MPTP/p-treated WT group or MPP$^+$-treated SH-SY5Y cells). NC, negative control; CTL, control. . (For interpretation of the references to colour in this figure legend, the reader is referred to the Web version of this article.)
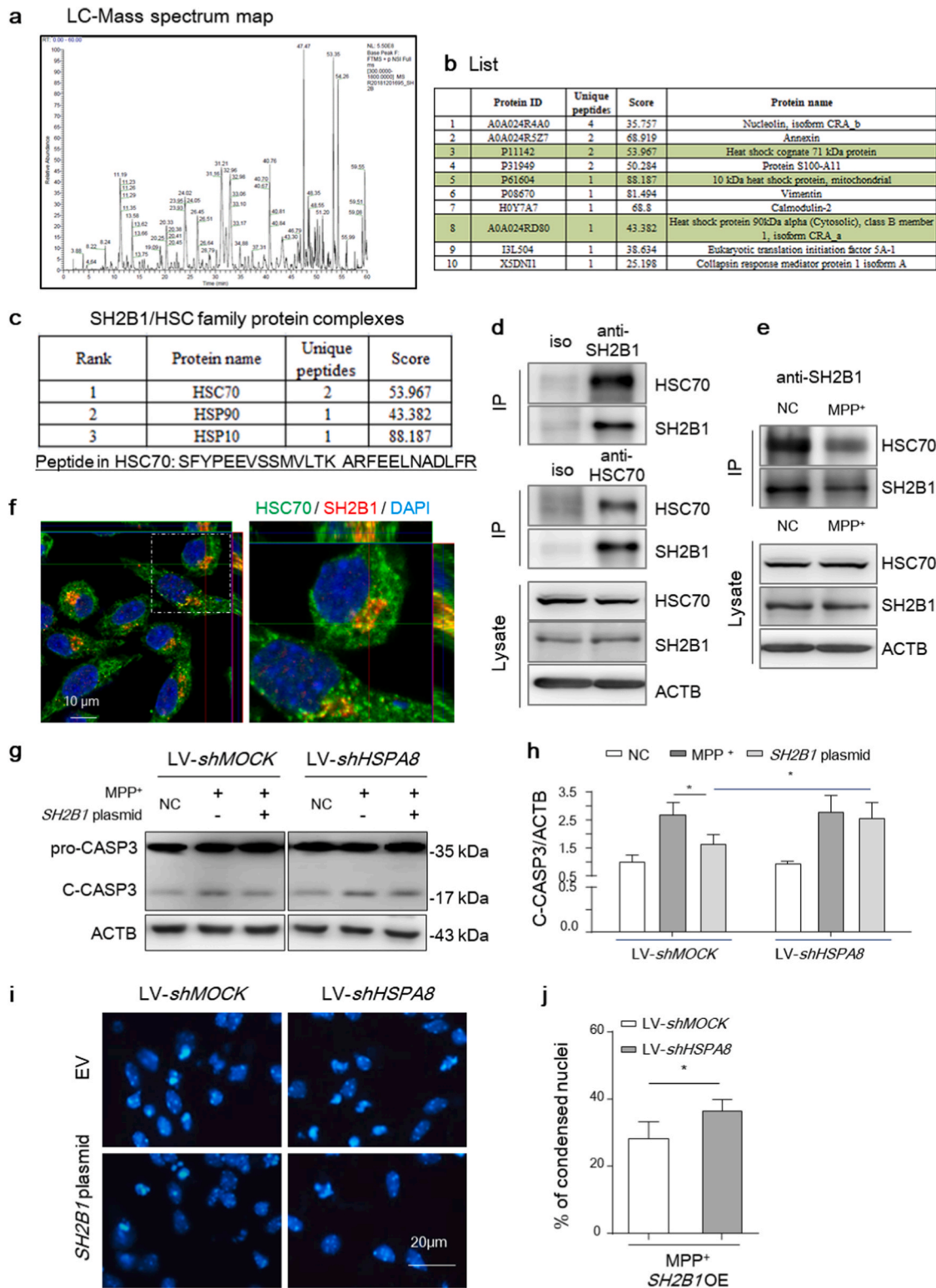
Fig. 4. SH2B1 directly binds to HSC70 and activates HSC70 pathway to attenuate SH-SY5Y cell apoptosis. (a and b) Base peak the LC-mass spectra of the SH2B1-bound proteins (a) and the proteins with the top 10 detected peptide hits in the mass spectrometry study (b). (c) SH2B1-bound proteins in SH-SY5Y cell lysates were identified by LC-MS/MS, and the bound heat shock family proteins are listed. (d) Cell lysates from SH-SY5Y cells were subjected to IP for SH2B1/HSC70, and eluted proteins were subjected to WB analysis using anti-HSC70 and anti-SH2B1 antibodies. (e) Lysates from control and MPP^+ (200 μM, 24 h)-stimulated SH-SY5Y cells were used for IP for SH2B1. (f) Confocal image showing the colocalization of SH2B1 and HSC70 in SH-SY5Y cells. Scale bar, 10 μm. (g–j) SH-SY5Y cells were co-transfected with *SH2B1* plasmid (or EV) and LV-*shHSPA8* (or LV-*shMOCK*) for 24 h and treated with (or without) MPP^+ for an additional 24 h. Cell lysates were extracted for immunoblot analysis of CASP3 (g and h) and fixed for Hoechst staining (i and j). Scale bar, 20 μm. All data are presented as the mean ± SEM. n = 3–4 per group in (g–j); three independent experiments. Analysed by (j) two-tailed Student's *t*-test or (h) one-way ANOVA with Tukey's post hoc test. *$P < 0.05$.
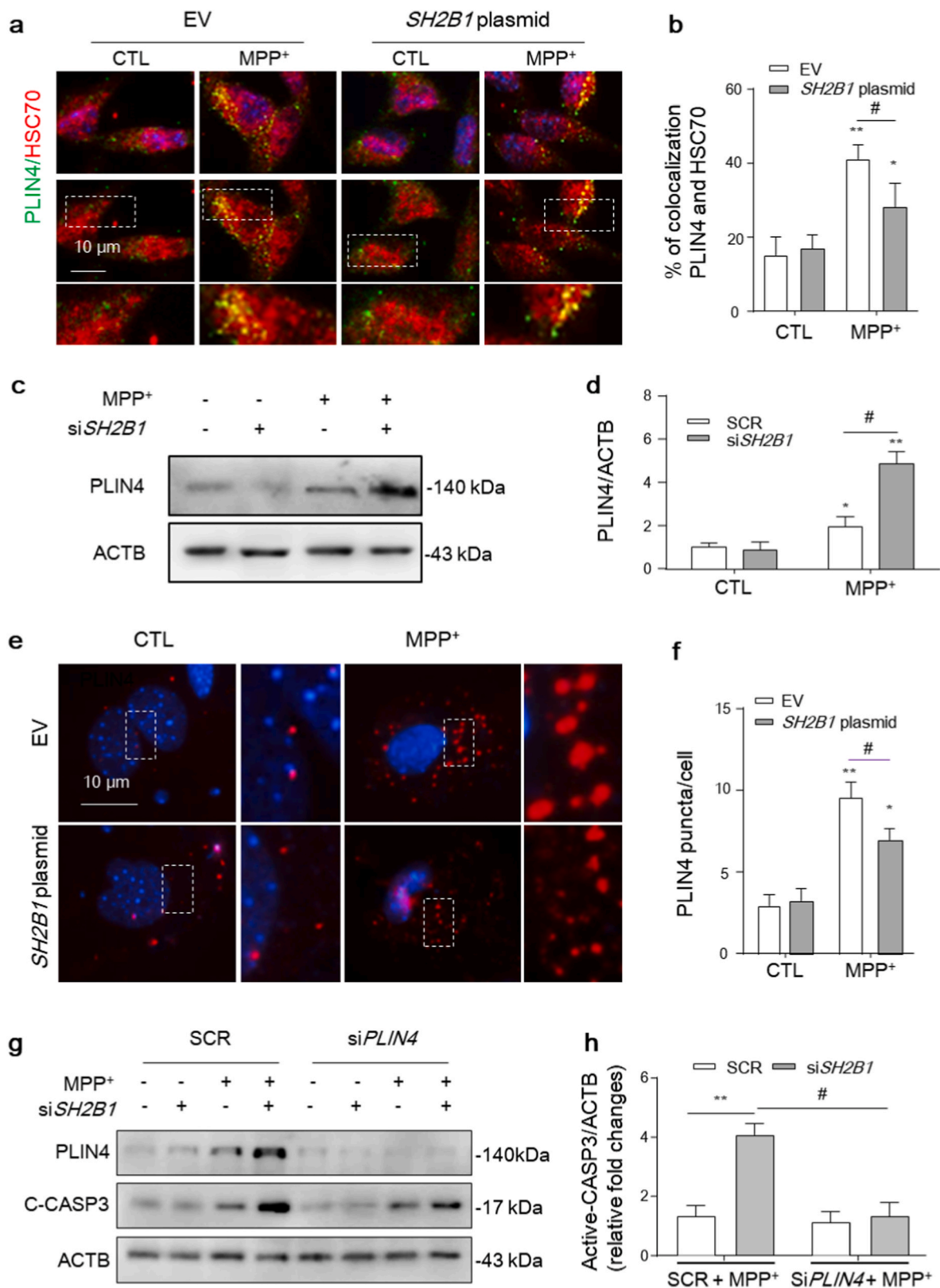
Fig. 5. SH2B1/HSC70/PLIN4 axis contributes to SH2B1-mediated neuroprotection. (a and b) SH-SY5Y cells were transfected with SH2B1 plasmid (or EV) for 24 h, stimulated with MPP$^+$ for another 24 h, and fixed for immunofluorescence staining of PLIN4 and HSC70. Scale bar, 10 μm. (c and d) SH-SY5Y cells were co-transfected with *SH2B1* siRNA (or SCR siRNA) for 24 h and treated with (or without) MPP$^+$ for an additional 24 h. Cell lysates were extracted for immunoblot analysis of PLIN4. (e and f) SH-SY5Y cells were infected with *SH2B1* plasmid (or EV) for 48 h and stimulated with MPP$^+$ for 24 h. Scale bar, 10 μm. (g and h) SH-SY5Y cells were co-transfected with *SH2B1* siRNA (or SCR siRNA) and *PLIN4* siRNA (or SCR siRNA) for 24 h and treated with (or without) MPP$^+$ for another 24 h. Cell lysates were extracted for WB analysis of PLIN4 and CASP3 expression. Data are presented as the mean ± SEM of three independent experiments. (a–h) n = 5–6 per group. Analysed by (b, d, f and h) one-way ANOVA with Tukey's post hoc test (*$P < 0.05$, **$P < 0.01$ versus vehicle; $^\#P < 0.05$ versus MPP$^+$ -treated cells; ns, not significant).
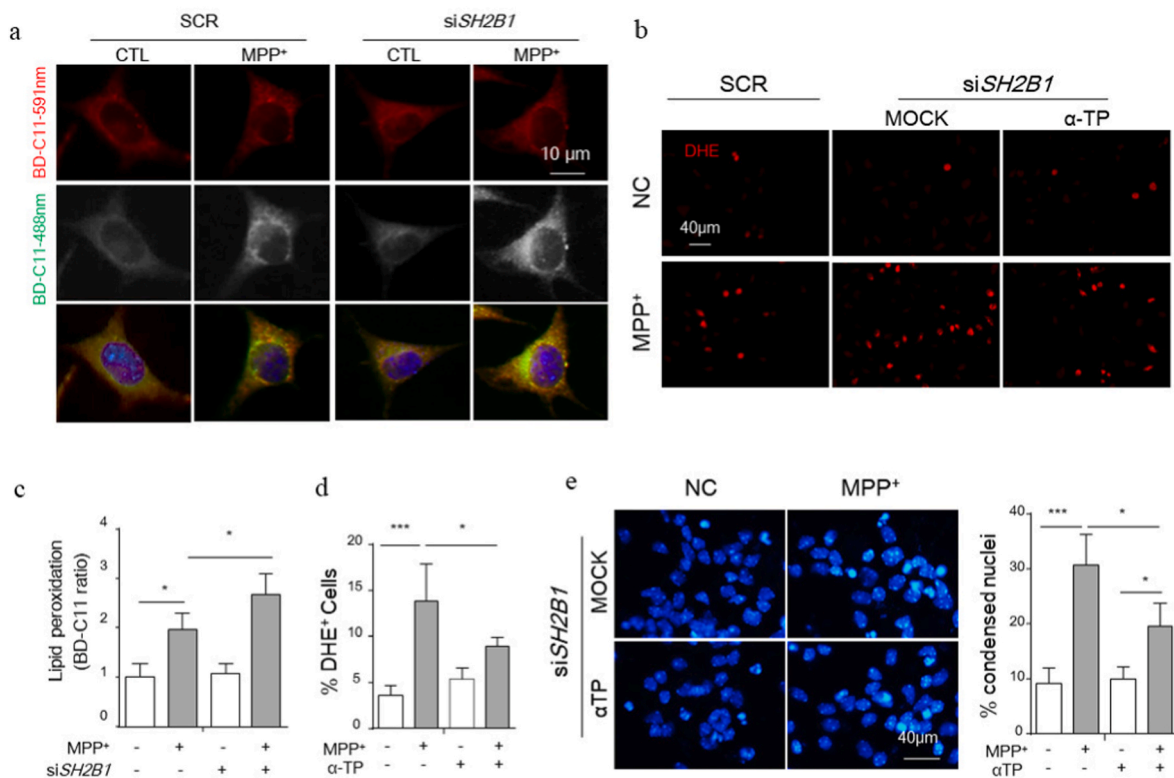
Fig. 6. Knockdown of *SH2B1* increases LD accumulation and exacerbates SH-SY5Y cell damage. (a and b) SH-SY5Y cells were transfected with *SH2B1* siRNA (or SCR siRNA) for 24 h, treated with or without 200 μM MPP$^+$ for 24 h, treated with 2 μM BODIPY$^{581/591}$ C11 for 1 h, and harvested for imaging to assess lipid peroxidation. Scale bar: (a) 10 μm, (b) 40 μm. (c–f) SH-SY5Y cells were transfected with *SH2B1* siRNA (or SCR siRNA) for 24 h and treated with or without 200 μM MPP$^+$ or 50 μM a-tocopherol for 24 h. The cells were incubated with DHE and fixed for imaging (c and d) to evaluate ROS stress (e and f). The same treated cells were fixed for Hoechst staining. Scale bar, 40 μm. Data are presented as the mean ± SEM of three independent experiments. (a–f) n = 5–6 per group. Analysed by (c, d and f) one-way ANOVA with Tukey's post hoc test (*$P < 0.05$, ***$P < 0.001$).

KO mice (Fig. 8c and d). LV-*Hspa8* injection could significantly decreased MPTP-induced accumulation of PLIN4 in WT controls but not in *Sh2b1* KO mice (Fig. 8c and d) by Western blot analysis. And immunofluorescence data also showed that LV-*Hspa8* injection decreased MPTP-induced accumulation of PLIN4 in WT controls but not in *Sh2b1* KO mice (Fig. 8e and f). The expression of genes (*Gpx8, Sod3, Cat, Acsbg1* and *Dbi*) involved in protecting against lipid toxicity and neutralizing lipids was significantly restored in WT LV-*Hspa8* injection group but not in *Sh2b1* KO mice (Fig. 8g). These results suggest that in the PD mouse model, enhancement of HSC70 activity can compensate for the MPTP-induced decrease in SH2B1 expression and PLIN4/LD/ROS-mediated stress; however, this compensatory mechanism might be in an SH2B1-dependent manner. This is consistent with the concept that SH2B1 interacts with HSC70 to form a complex that interdependently regulates the degradation of the substrate PLIN4.

4. Discussion

Although our works and the research of other groups have confirmed that SH2B1 plays a metabolic role and intensive studies have revealed that metabolic dysfunction is a risk factor for neurodegenerative diseases, there has been limited research on the role of SH2B1 in the pathogenesis of neurodegenerative diseases, especially PD. This study provides the first evidence that *Sh2b1* deficiency markedly exacerbates behavioural defects and increases neuronal apoptosis in MPTP/p-treated mice, whereas restoration of *Sh2b1* expression, especially in neurons, significantly reverses these negative effects, suggesting that *Sh2b1* is a physiological protective factor against PD in mice. In support of this notion, SH2B1 expression was confirmed to be downregulated in the blood samples of PD patients and in the brains of mice with MPTP/p-induced chronic PD.

SH2B1 is a newly identified key regulator of body weight and glucose metabolism [10,29]. Several studies have independently reported that single-nucleotide polymorphisms within the human *SH2B1* loci are genetically linked to leptin resistance and obesity [30,31]. Disruption of the Drosophila *Sh2b1* homologue also increases lipid accumulation and fat content in flies [7]. Therefore, SH2B1 plays a key and conserved role in the control of energy and glucose metabolism in insects, rodents, and humans. Moreover, Ren et al. [8] observed that neuron-specific restoration of *Sh2b1* expression alleviates hyperphagia, obesity, and T2D in *Sh2b1*-null mice, further confirming that neuronal SH2B1 is essential in regulating systemic energy balance. SH2B1 can bind to both the insulin receptor and insulin receptor substrate (IRS) proteins [32,33] to enhance insulin/insulin-like growth factor-1 signalling (IIS) by promoting IRS phosphorylation or by preventing IRS dephosphorylation [33]. On the other hand, some studies have reported that systemic metabolic abnormalities are risk factors for PD, and that at the cellular level, enhancement of IRS signals can promote neuronal survival under various stresses [6,34–36]. Thus, we hypothesised that SH2B1 might exert a neuroprotective effect against PD through the regulation of metabolic processes.

This study demonstrated that SH2B1 is expressed at relatively high levels in the midbrain and striatum, mostly in TH$^+$ neurons, under basal conditions and that SH2B1 expression is significantly reduced in the PD mouse model. The loss of DA neurons was further associated with an MPTP-dependent increase in apoptotic cell death in the mouse brain, as shown by significant increases in the numbers of active CASP3$^+$ and TUNEL$^+$ cells in the SNpc of both MPTP-treated WT mice and *Sh2b1* KO mice. Lastly, AAV-mediated *Sh2b1* overexpression, which restored SH2B1 expression specifically in neurons, reversed MPTP-induced
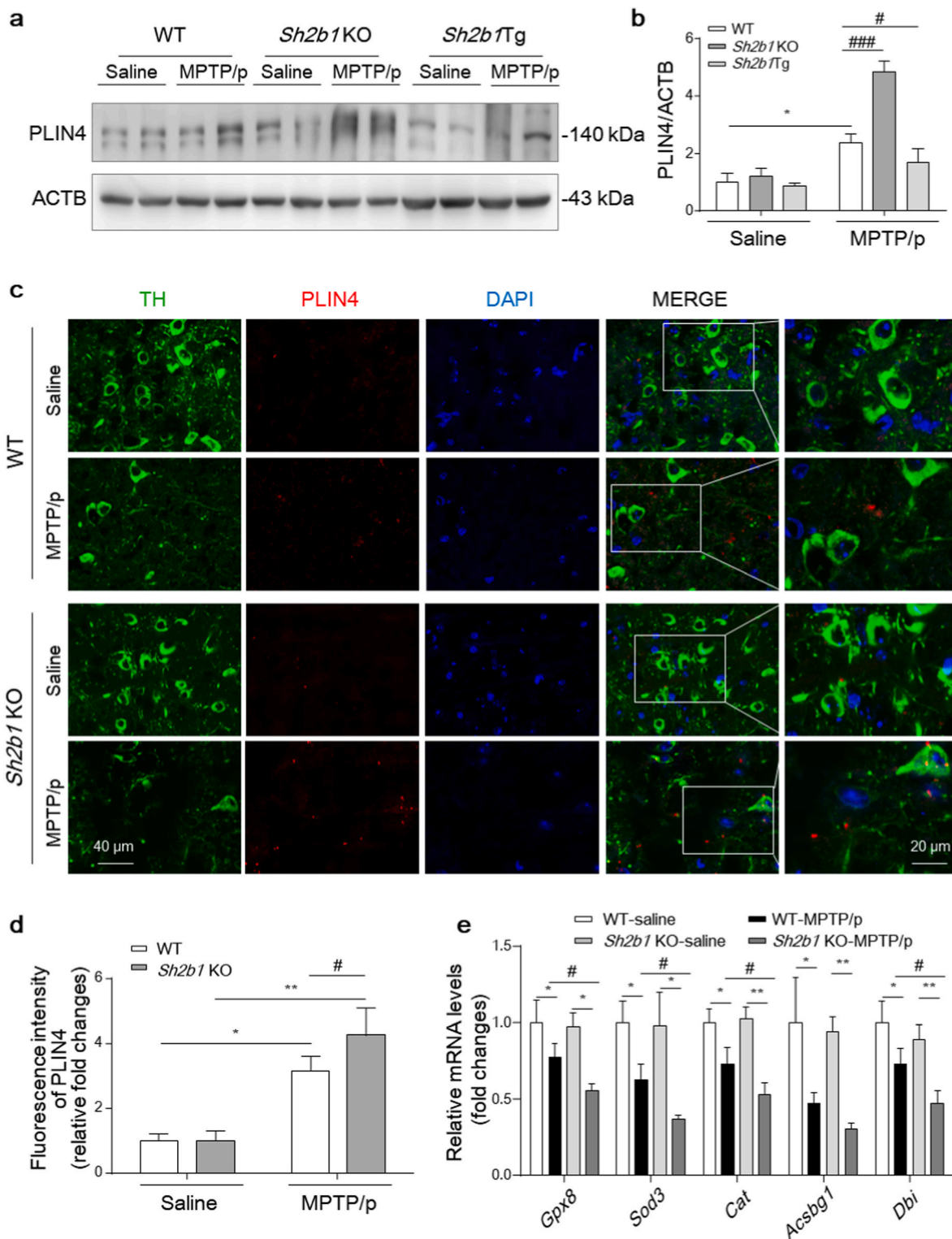
Fig. 7. SH2B1 deficiency inhibits PLIN4 degradation and increases LD accumulation in MPTP/p-induced PD mice. (a and b) WB analysis of PLIN4 expression in the midbrains of the indicated mice. (c and d) Immunofluorescence staining for PLIN4 and TH and co-staining for PLIN4/TH of the midbrain segments and quantitation of PLIN4 fluorescence intensity. Scale bar, 40/20 μm. (e) qPCR analysis of *Gpx8*, *Sod3*, *Cat*, *Acsbg1* and *Dbi* mRNA levels in the mouse SNpc. Data are presented as the mean ± SEM of three independent experiments. (a–e) n = 4–5 per group. Analysed by (b, d and e) one-way ANOVA with Tukey's post hoc test (*P < 0.05, **P < 0.05 versus saline group; #P < 0.05, ###P < 0.001 versus MPTP/p-treated WT group).

neurotoxicity in *Sh2b1* KO mice. Moreover, we found that *SH2B1* silencing significantly increased MPP + -induced SH-SY5Y cell apoptosis, whereas its overexpression inhibits MPP + -induced cell apoptosis *in vitro*.

As an adaptor protein, intracellular SH2B1 can bind to a series of proteins, including IRS [37] and Janus kinase 2 (JAK2) [38]. To identify the protein interacting with SH2B1, we immunoprecipitated SH2B1, including its bound proteins, from cultured SH-SY5Y cells for MS
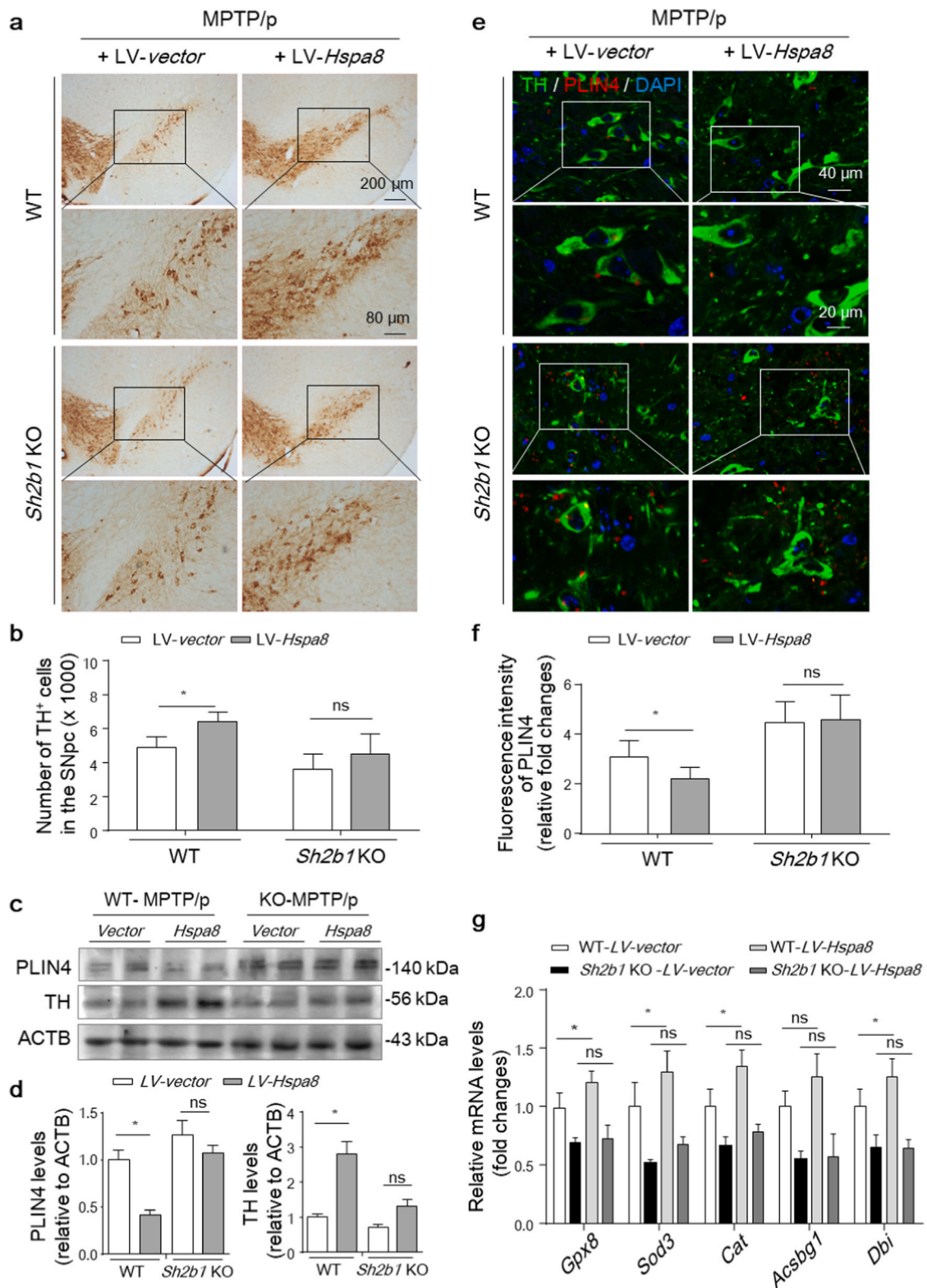
Fig. 8. Restoration of neuronal *Hspa8* expression alleviates MPTP-induced neurodegeneration in an SH2B1 dependent manner. (a and b) Representative images and quantification of TH+ neurons in each group. Scale bar, 200/80 μm. (c and d) WB analysis and quantification of TH and PLIN4 levels in the mouse SNpc. (e and f) Representative images of PLIN4 (red) and TH (green) coimmunostaining and quantification of PLIN4+ neurons in the SNpc of WT and *Sh2b1* KO mice after LV-*Hspa8* (or LV-*vector*) microinjection followed by MPTP/p insult. Scale bar, 40/20 μm. (g) qPCR analysis of *Gpx8*, *Sod3*, *Cat*, *Acsbg1* and *Dbi* mRNA expression in the mouse SNpc. Data are presented as the mean ± SEM three independent experiments. (a–g) n = 4–6 per group. Analysed by (b, d, f and g) one-way ANOVA with Tukey's post hoc test (*$P < 0.05$; *ns,* no significance). . (For interpretation of the references to colour in this figure legend, the reader is referred to the Web version of this article.)

analysis and found that HSC70 can interact with SH2B1. The ability of SH2B1 to bind to HSC70 was further confirmed *in vitro* by immuno-precipitation and fluorescence colocalization analysis. This finding provides novel insights into the biological functions of HSC70 and the role of SH2B1 in PD. The protein HSPA8/HSC70, a constitutively expressed cognate protein of the HSP70 family, is an interesting chaperone protein [39]. Through its cooperation with co-chaperones, HSP70 plays a conserved role in various cellular functions, including clathrin-mediated endocytosis [40], protein folding, and regulation of autophagy mediated by chaperones (chaperone-mediated autophagy [CMA]) [39,41,42]. In this study, the neuroprotective effects of SH2B1 against MPP$^+$ were mostly blunted by *HSC70* silencing, suggesting that SH2B1's function in neurons involves HSC70. HSC70 has long been proposed to be associated with PD [43,44], as α-synuclein is a proven substrate of HSC70 [45,46].

Using a KFERQ-finder computational tool, we identified PLIN4 (an LD-associated protein) as a substrate of SH2B1/HSC70 in PD. Kaushik and Cuervo et al. [47] first reported that the LD-associated proteins PLIN2 and PLIN3 are CMA substrates and that their degradation via CMA promotes LD breakdown and precedes lipolysis in hepatocytes. Increased accumulation of LDs in the subventricular zone (SVZ) was noted in mouse models of AD and human AD patients [48]. Previously, we have sequenced mesencephalon samples and reported that PLIN4 levels and the number of LDs are increased in PD mice. Mechanistically, lipid accumulation in cells is related to mitochondrial dysfunction and impaired FA oxidation [21]. Based on these findings, we speculate that when lipids are overloaded, insulted cells cannot effectively metabolise them, resulting in lipid peroxidation, increased ROS stress, and the induction of cellular apoptosis. In this study, we revealed PLIN4, which can be recognised by HSC70, as an LD-associated protein. SH2B1 increases the binding of PLIN4 by HSC70. Functionally, these alterations enhance the degradation of PLIN4 by HSC70, reducing LD accumulation and oxidative stress in neurons.

This study had some limitations. First, as a key regulator of CMA process, HSC70 can recognise and guide specific substrates to lysosome for degradation in an macroautophagy-independent way [47,49]. However, the detailed mechanism by which SH2B1 regulates the CMA–lysosomal pathway remains unclear and requires further investigation. Second, as we have previously demonstrated, the intact SH2 domain of SH2B1 is required; however, the SH2domain of SH2B1 alone was unable to maintain glucose homeostasis in mice. Thus, the structure and domain responsible for HSC70 binding should be identified. Although the HSC70–CMA pathway is likely to mediate the pro-survival effects of SH2B1 in DA neurons, our data do not exclude the possibility that SH2B1 protects against neurodegeneration in PD by other mechanisms.

Additionally, comprehensive strategies of 'brain energy rescue' have been proposed as promising treatment for neurodegenerative diseases, including PD [50]. Among these approaches, rescuing declined glucose metabolism through increasing insulin sensitivity, reinstating glycolysis and oxidative phosphorylation, and rectifying mitochondrial dysfunction is of great importance for PD therapy [51]. Abnormal glucose tolerance and insulin resistance are prevalent in both glial cells and neurons in PD patients [6], while activating insulin signaling such as IGF1-related pathway ameliorates PD pathology [6,52]. Although beneficial effects of SH2B1 enhancement have not been clarified in PD research, the regulatory role of SH2B1 in glucose metabolism has been well established in the peripheral and central nervous systems, contributing to insulin sensitivity, insulin signalling pathways and energy homeostasis [8,14,37]. Therefore, a full picture of the translational potential of SH2B1 alteration for PD therapy in future might provide a prospective therapeutic idea through restoring glucose metabolism in both glial cells and neurons.

Availability of data and materials

The datasets used and/or analysed in the current study are available from the corresponding authors on reasonable request.

Authors' contributions

G.H. and J.H. designed the experiments. X.H., Y.L., Y.D., T.X., Q.H., X.Y., L.R., and J.H. performed the experiments. X.H., Y.L., L.R., and J.H. analysed and interpreted the data from experiments. All authors discussed the results and commented on the manuscript.

Declarations of competing interest

None.

References

[1] A. Grunewald, K.R. Kumar, C.M. Sue, New insights into the complex role of mitochondria in Parkinson's disease, Prog. Neurobiol. 177 (2019) 73–93, https://doi.org/10.1016/j.pneurobio.2018.09.003.

[2] W. Poewe, K. Seppi, C.M. Tanner, G.M. Halliday, P. Brundin, J. Volkmann, A. E. Schrag, A.E. Lang, Parkinson disease, Nat. Rev. Dis. Prim. 3 (2017) 17013, https://doi.org/10.1038/nrdp.2017.13.

[3] J.A. Santiago, J.A. Potashkin, Shared dysregulated pathways lead to Parkinson's disease and diabetes, Trends Mol. Med. 19 (2013) 176–186, https://doi.org/10.1016/j.molmed.2013.01.002.

[4] R. Fernandez-Santiago, A. Esteve-Codina, M. Fernandez, F. Valldeoriola, A. Sanchez-Gomez, E. Munoz, Y. Compta, E. Tolosa, M. Ezquerra, M.J. Marti, Transcriptome analysis in LRRK2 and idiopathic Parkinson's disease at different glucose levels, NPJ Parkinsons Dis. 7 (2021) 109, https://doi.org/10.1038/s41531-021-00255-x.

[5] W. Liu, J. Tang, Association between diabetes mellitus and risk of Parkinson's disease: a prisma-compliant meta-analysis, Brain Behav. 11 (2021), e02082, https://doi.org/10.1002/brb3.2082.

[6] D. Athauda, T. Foltynie, Insulin resistance and Parkinson's disease: a new target for disease modification? Prog. Neurobiol. 145–146 (2016) 98–120, https://doi.org/10.1016/j.pneurobio.2016.10.001.

[7] W. Song, D. Ren, W. Li, L. Jiang, K.W. Cho, P. Huang, C. Fan, Y. Song, Y. Liu, L. Rui, SH2B regulation of growth, metabolism, and longevity in both insects and mammals, Cell Metabol. 11 (2010) 427–437, https://doi.org/10.1016/j.cmet.2010.04.002.

[8] D. Ren, Y. Zhou, D. Morris, M. Li, Z. Li, L. Rui, Neuronal SH2B1 is essential for controlling energy and glucose homeostasis, J. Clin. Invest. 117 (2007) 397–406, https://doi.org/10.1172/JCI29417.

[9] L. Rui, C. Carter-Su, Identification of SH2-bbeta as a potent cytoplasmic activator of the tyrosine kinase Janus kinase 2, Proc. Natl. Acad. Sci. U. S. A. 96 (1999) 7172–7177, https://doi.org/10.1073/pnas.96.13.7172.

[10] D. Ren, M. Li, C. Duan, L. Rui, Identification of SH2-B as a key regulator of leptin sensitivity, energy balance, and body weight in mice, Cell Metabol. 2 (2005) 95–104, https://doi.org/10.1016/j.cmet.2005.07.004.

[11] M. Li, D. Ren, M. Iseki, S. Takaki, L. Rui, Differential role of SH2-B and APS in regulating energy and glucose homeostasis, Endocrinology 147 (2006) 2163–2170, https://doi.org/10.1210/en.2005-1313.

[12] Y.C. Hsu, S.L. Chen, Y.J. Wang, Y.H. Chen, D.Y. Wang, L. Chen, C.H. Chen, H. H. Chen, I.M. Chiu, Signaling adaptor protein SH2B1 enhances neurite outgrowth and accelerates the maturation of human induced neurons, Stem Cell. Transl. Med. 3 (2014) 713–722, https://doi.org/10.5966/sctm.2013-0111.

[13] C. Slack, C. Werz, D. Wieser, N. Alic, A. Foley, H. Stocker, D.J. Withers, J. M. Thornton, E. Hafen, L. Partridge, Regulation of lifespan, metabolism, and stress responses by the Drosophila SH2B protein, Lnk, PLoS Genet. 6 (2010), e1000881, https://doi.org/10.1371/journal.pgen.1000881.

[14] S. Wang, Y. Cheng, Y. Gao, Z. He, W. Zhou, R. Chang, Z. Peng, Y. Zheng, C. Duan, C. Zhang, SH2B1 promotes epithelial-mesenchymal transition through the IRS1/beta-catenin signaling axis in lung adenocarcinoma, Mol. Carcinog. 57 (2018) 640–652, https://doi.org/10.1002/mc.22788.

[15] Y. Shen, Y. Xia, S. Meng, N.K. Lim, W. Wang, F. Huang, SH2B1 is involved in the accumulation of amyloid-beta42 in Alzheimer's disease, J. Alzheimers Dis. 55 (2017) 835–847, https://doi.org/10.3233/JAD-160233.

[16] L. Jiang, H. Su, X. Wu, H. Shen, M.H. Kim, Y. Li, M.G. Myers Jr., C. Owyang, L. Rui, Leptin receptor-expressing neuron Sh2b1 supports sympathetic nervous system and protects against obesity and metabolic disease, Nat. Commun. 11 (2020) 1517, https://doi.org/10.1038/s41467-020-15328-3.

[17] L. Jiang, H. Su, J.M. Keogh, Z. Chen, E. Henning, P. Wilkinson, I. Goodyer, I. S. Farooqi, L. Rui, Neural deletion of Sh2b1 results in brain growth retardation and reactive aggression, Faseb. J. 32 (2018) 1830–1840, https://doi.org/10.1096/fj.201700831R.

[18] Y. Liu, X. Zeng, Y. Hui, C. Zhu, J. Wu, D.H. Taylor, J. Ji, W. Fan, Z. Huang, J. Hu, Activation of alpha7 nicotinic acetylcholine receptors protects astrocytes against oxidative stress-induced apoptosis: implications for Parkinson's disease, Neuropharmacology 91 (2015) 87–96, https://doi.org/10.1016/j.neuropharm.2014.11.028.

[19] Y. Liu, J. Hu, J. Wu, C. Zhu, Y. Hui, Y. Han, Z. Huang, K. Ellsworth, W. Fan, alpha7 nicotinic acetylcholine receptor-mediated neuroprotection against dopaminergic neuron loss in an MPTP mouse model via inhibition of astrocyte activation, J. Neuroinflammation 9 (2012) 98, https://doi.org/10.1186/1742-2094-9-98.

[20] Y. Liu, S. Hao, B. Yang, Y. Fan, X. Qin, Y. Chen, J. Hu, Wnt/beta-catenin signaling plays an essential role in alpha7 nicotinic receptor-mediated neuroprotection of dopaminergic neurons in a mouse Parkinson's disease model, Biochem. Pharmacol. 140 (2017) 115–123, https://doi.org/10.1016/j.bcp.2017.05.017.

[21] X. Han, J. Zhu, X. Zhang, Q. Song, J. Ding, M. Lu, S. Sun, G. Hu, Plin4-Dependent lipid droplets hamper neuronal mitophagy in the MPTP/p-Induced mouse model of Parkinson's disease, Front. Neurosci. 12 (2018) 397, https://doi.org/10.3389/fnins.2018.00397.

[22] X. Han, S. Sun, Y. Sun, Q. Song, J. Zhu, N. Song, M. Chen, T. Sun, M. Xia, J. Ding, M. Lu, H. Yao, G. Hu, Small molecule-driven NLRP3 inflammation inhibition via interplay between ubiquitination and autophagy: implications for Parkinson disease, Autophagy 15 (2019) 1860–1881, https://doi.org/10.1080/15548627.2019.1596481.

[23] J. Zhu, Z. Hu, X. Han, D. Wang, Q. Jiang, J. Ding, M. Xiao, C. Wang, M. Lu, G. Hu, Dopamine D2 receptor restricts astrocytic NLRP3 inflammasome activation via enhancing the interaction of beta-arrestin2 and NLRP3, Cell Death Differ. 25 (2018) 2037–2049, https://doi.org/10.1038/s41418-018-0127-2.

[24] Y. Wei, M. Lu, M. Mei, H. Wang, Z. Han, M. Chen, H. Yao, N. Song, X. Ding, J. Ding, M. Xiao, G. Hu, Pyridoxine induces glutathione synthesis via PKM2-mediated Nrf2 transactivation and confers neuroprotection, Nat. Commun. 11 (2020) 941, https://doi.org/10.1038/s41467-020-14788-x.

[25] L. Brichta, W. Shin, V. Jackson-Lewis, J. Blesa, E.L. Yap, Z. Walker, J. Zhang, J. P. Roussarie, M.J. Alvarez, A. Califano, S. Przedborski, P. Greengard, Identification of neurodegenerative factors using translatome-regulatory network analysis, Nat. Neurosci. 18 (2015) 1325–1333, https://doi.org/10.1038/nn.4070.

[26] X. Han, S. Zhao, H. Song, T. Xu, Q. Fang, G. Hu, L. Sun, Kaempferol alleviates LD-mitochondrial damage by promoting autophagy: implications in Parkinson's disease, Redox Biol. 41 (2021) 101911, https://doi.org/10.1016/j.redox.2021.101911.

[27] G.F. Grabner, H. Xie, M. Schweiger, R. Zechner, Lipolysis: cellular mechanisms for lipid mobilization from fat stores, Nat. Metab. 3 (2021) 1445–1465, https://doi.org/10.1038/s42255-021-00493-6.

[28] A.R. Kimmel, C. Sztalryd, The perilipins: major cytosolic lipid droplet-associated proteins and their roles in cellular lipid storage, mobilization, and systemic homeostasis, Annu. Rev. Nutr. 36 (2016) 471–509, https://doi.org/10.1146/annurev-nutr-071813-105410.

[29] D.L. Morris, L. Rui, Recent advances in understanding leptin signaling and leptin resistance, Am. J. Physiol. Endocrinol. Metab. 297 (2009) E1247–E1259, https://doi.org/10.1152/ajpendo.00274.2009.

[30] G. Thorleifsson, G.B. Walters, D.F. Gudbjartsson, V. Steinthorsdottir, P. Sulem, A. Helgadottir, U. Styrkarsdottir, S. Gretarsdottir, S. Thorlacius, I. Jonsdottir, T. Jonsdottir, E.J. Olafsdottir, G.H. Olafsdottir, T. Jonsson, F. Jonsson, K. Borch-Johnsen, T. Hansen, G. Andersen, T. Jorgensen, T. Lauritzen, K.K. Aben, A. L. Verbeek, N. Roeleveld, E. Kampman, L.R. Yanek, L.C. Becker, L. Tryggvadottir, T. Rafnar, D.M. Becker, J. Gulcher, L.A. Kiemeney, O. Pedersen, A. Kong, U. Thorsteinsdottir, K. Stefansson, Genome-wide association yields new sequence variants at seven loci that associate with measures of obesity, Nat. Genet. 41 (2009) 18–24, https://doi.org/10.1038/ng.274.

[31] C.J. Willer, E.K. Speliotes, R.J. Loos, S. Li, C.M. Lindgren, I.M. Heid, S.I. Berndt, A. L. Elliott, A.U. Jackson, C. Lamina, G. Lettre, N. Lim, H.N. Lyon, S.A. McCarroll, K. Papadakis, L. Qi, J.C. Randall, R.M. Roccasecca, S. Sanna, P. Scheet, M. N. Weedon, E. Wheeler, J.H. Zhao, L.C. Jacobs, I. Prokopenko, N. Soranzo, T. Tanaka, N.J. Timpson, P. Almgren, A. Bennett, R.N. Bergman, S.A. Bingham, L. L. Bonnycastle, M. Brown, N.P. Burtt, P. Chines, L. Coin, F.S. Collins, J.M. Connell, C. Cooper, G.D. Smith, E.M. Dennison, P. Deodhar, P. Elliott, M.R. Erdos, K. Estrada, D.M. Evans, L. Gianniny, C. Gieger, C.J. Gillson, C. Guiducci, R. Hackett, D. Hadley, A.S. Hall, A.S. Havulinna, J. Hebebrand, A. Hofman, B. Isomaa, K.B. Jacobs, T. Johnson, P. Jousilahti, Z. Jovanovic, K.T. Khaw, P. Kraft,

M. Kuokkanen, J. Kuusisto, E.G. Lakatta, J. Luan, R.N. Luben, M. Mangino, W.L. McArdle, T. Meitinger, A. Mulas, P.B. Munroe, N. Narisu, A. R. Ness, K. Northstone, S. O'Rahilly, C. Purmann, M.G. Rees, M. Ridderstrale, S. M. Ring, F. Rivadeneira, A. Ruokonen, M.S. Sandhu, J. Saramies, L.J. Scott, A. Scuteri, K. Silander, M.A. Sims, K. Song, J. Stephens, S. Stevens, H.M. Stringham, Y.C. Tung, T.T. Valle, C.M. van Duijn, K.S. Vimaleswaran, P. Vollenweider, G. Waeber, C. Wallace, R.M. Watanabe, D.M. Waterworth, N. Watkins, C. Wellcome Trust Case Control, J.C. Witteman, E. Zeggini, G. Zhai, M.C. Zillikens, D. Altshuler, M.J. Caulfield, S.J. Chanock, I.S. Farooqi, L. Ferrucci, J.M. Guralnik, A.T. Hattersley, F.B. Hu, M.R. Jarvelin, M. Laakso, V. Mooser, K.K. Ong, W. H. Ouwehand, V. Salomaa, N.J. Samani, T.D. Spector, T. Tuomi, J. Tuomilehto, M. Uda, A.G. Uitterlinden, N.J. Wareham, P. Deloukas, T.M. Frayling, L.C. Groop, R.B. Hayes, D.J. Hunter, K.L. Mohlke, L. Peltonen, D. Schlessinger, D.P. Strachan, H.E. Wichmann, M.I. McCarthy, M. Boehnke, I. Barroso, G.R. Abecasis, J. N. Hirschhorn, T.C. An, Genetic Investigation of, Six new loci associated with body mass index highlight a neuronal influence on body weight regulation, Nat. Genet. 41 (2009) 25–34, https://doi.org/10.1038/ng.287.

[32] C. Duan, M. Li, L. Rui, SH2-B promotes insulin receptor substrate 1 (IRS1)- and IRS2-mediated activation of the phosphatidylinositol 3-kinase pathway in response to leptin, J. Biol. Chem. 279 (2004) 43684–43691, https://doi.org/10.1074/jbc.M408495200.

[33] D.L. Morris, K.W. Cho, Y. Zhou, L. Rui, SH2B1 enhances insulin sensitivity by both stimulating the insulin receptor and inhibiting tyrosine dephosphorylation of insulin receptor substrate proteins, Diabetes 58 (2009) 2039–2047, https://doi.org/10.2337/db08-1388.

[34] A. Abdullah, N. Mohd Murshid, S. Makpol, Antioxidant modulation of mTOR and sirtuin pathways in age-related neurodegenerative diseases, Mol. Neurobiol. 57 (2020) 5193–5207, https://doi.org/10.1007/s12035-020-02083-1.

[35] H.M. Chow, M. Shi, A. Cheng, Y. Gao, G. Chen, X. Song, R.W.L. So, J. Zhang, K. Herrup, Age-related hyperinsulinemia leads to insulin resistance in neurons and cell-cycle-induced senescence, Nat. Neurosci. 22 (2019) 1806–1819, https://doi.org/10.1038/s41593-019-0505-1.

[36] V.R. Muddapu, S.A.P. Dharshini, V.S. Chakravarthy, M.M. Gromiha, Neurodegenerative diseases - is metabolic deficiency the root cause? Front. Neurosci. 14 (2020) 213, https://doi.org/10.3389/fnins.2020.00213.

[37] L. Rui, SH2B1 regulation of energy balance, body weight, and glucose metabolism, World J. Diabetes 5 (2014) 511–526, https://doi.org/10.4239/wjd.v5.i4.511.

[38] T.J. Maures, J.H. Kurzer, C. Carter-Su, SH2B1 (SH2-B) and JAK2: a multifunctional adaptor protein and kinase made for each other, Trends Endocrinol. Metab. 18 (2007) 38–45, https://doi.org/10.1016/j.tem.2006.11.007.

[39] F. Stricher, C. Macri, M. Ruff, S. Muller, HSPA8/HSC70 chaperone protein: structure, function, and chemical targeting, Autophagy 9 (2013) 1937, https://doi.org/10.4161/auto.26448, 1954.

[40] T.G. Chappell, W.J. Welch, D.M. Schlossman, K.B. Palter, M.J. Schlesinger, J. E. Rothman, Uncoating ATPase is a member of the 70 kilodalton family of stress proteins, Cell 45 (1986) 3–13, https://doi.org/10.1016/0092-8674(86)90532-5.

[41] S. Kaushik, A.M. Cuervo, The coming of age of chaperone-mediated autophagy, Nat. Rev. Mol. Cell Biol. 19 (2018) 365–381, https://doi.org/10.1038/s41580-018-0001-6.

[42] T. Liu, C.K. Daniels, S. Cao, Comprehensive review on the HSC70 functions, interactions with related molecules and involvement in clinical diseases and therapeutic potential, Pharmacol. Ther. 136 (2012) 354–374, https://doi.org/10.1016/j.pharmthera.2012.08.014.

[43] R. San Gil, L. Ooi, J.J. Yerbury, H. Ecroyd, The heat shock response in neurons and astroglia and its role in neurodegenerative diseases, Mol. Neurodegener. 12 (2017) 65, https://doi.org/10.1186/s13024-017-0208-6.

[44] R. Yang, G. Gao, Z. Mao, Q. Yang, Chaperone-mediated autophagy and mitochondrial homeostasis in Parkinson's disease, Parkinsons Dis. (2016) 2613401, https://doi.org/10.1155/2016/2613401, 2016.

[45] M. Martinez-Vicente, Z. Talloczy, S. Kaushik, A.C. Massey, J. Mazzulli, E. v Mosharov, R. Hodara, R. Fredenburg, D.C. Wu, A. Follenzi, W. Dauer, S. Przedborski, H. Ischiropoulos, P.T. Lansbury, D. Sulzer, A.M. Cuervo, Dopamine-modified alpha-synuclein blocks chaperone-mediated autophagy, J. Clin. Invest. 118 (2008) 777–788, https://doi.org/10.1172/JCI32806.

[46] C. Roodveldt, C.W. Bertoncini, A. Andersson, A.T. van der Goot, S.T. Hsu, R. Fernandez-Montesinos, J. de Jong, T.J. van Ham, E.A. Nollen, D. Pozo, J. Christodoulou, C.M. Dobson, Chaperone proteostasis in Parkinson's disease: stabilization of the Hsp70/alpha-synuclein complex by Hip, EMBO J. 28 (2009) 3758–3770, https://doi.org/10.1038/emboj.2009.298.

[47] S. Kaushik, A.M. Cuervo, Degradation of lipid droplet-associated proteins by chaperone-mediated autophagy facilitates lipolysis, Nat. Cell Biol. 17 (2015) 759–770, https://doi.org/10.1038/ncb3166.

[48] L.K. Hamilton, M. Dufresne, S.E. Joppe, S. Petryszyn, A. Aumont, F. Calon, F. Barnabe-Heider, A. Furtos, M. Parent, P. Chaurand, K.J. Fernandes, Aberrant lipid metabolism in the forebrain niche suppresses adult neural stem cell proliferation in an animal model of Alzheimer's disease, Cell Stem Cell 17 (2015) 397–411, https://doi.org/10.1016/j.stem.2015.08.001.

[49] P.W. Ho, C.T. Leung, H. Liu, S.Y. Pang, C.S. Lam, J. Xian, L. Li, M.H. Kung, D. B. Ramsden, S.L. Ho, Age-dependent accumulation of oligomeric SNCA/alpha-synuclein from impaired degradation in mutant LRRK2 knockin mouse model of Parkinson disease: role for therapeutic activation of chaperone-mediated autophagy (CMA), Autophagy 16 (2020) 347–370, https://doi.org/10.1080/15548627.2019.1603545.

[50] J.S. Chu, T.H. Liu, K.L. Wang, C.L. Han, Y.P. Liu, S. Michitomo, J.G. Zhang, T. Fang, F.G. Meng, The metabolic activity of caudate and prefrontal cortex negatively

correlates with the severity of idiopathic Parkinson's disease, Aging Dis. 10 (2019) 847–853, https://doi.org/10.14336/AD.2018.0814.

[51] S.C. Cunnane, E. Trushina, C. Morland, A. Prigione, G. Casadesus, Z.B. Andrews, M. F. Beal, L.H. Bergersen, R.D. Brinton, S. de la Monte, A. Eckert, J. Harvey, R. Jeggo, J.H. Jhamandas, O. Kann, C.M. la Cour, W.F. Martin, G. Mithieux, P.I. Moreira, M. P. Murphy, K.A. Nave, T. Nuriel, S.H.R. Oliet, F. Saudou, M.P. Mattson, R. H. Swerdlow, M.J. Millan, Brain energy rescue: an emerging therapeutic concept for neurodegenerative disorders of ageing, Nat. Rev. Drug Discov. 19 (2020) 609–633, https://doi.org/10.1038/s41573-020-0072-x.

[52] M. Ramalingam, S.J. Kim, Protective effects of activated signaling pathways by insulin on C6 glial cell model of MPP(+)-induced Parkinson's disease, J. Recept. Signal Transduct. Res. 37 (2017) 100–107, https://doi.org/10.3109/ 10799893.2016.1171342.